NASA TN D-1513

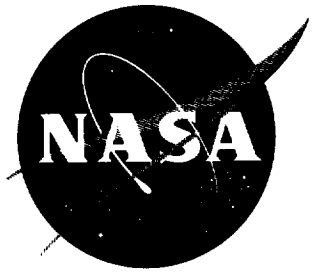

TECHNICAL NOTE

D-1513

BUCKLING OF RING-STIFFENED CYLINDERS UNDER A PURE BENDING MOMENT AND A NONUNIFORM TEMPERATURE DISTRIBUTION

By Melvin S. Anderson and Michael F. Card

Langley Research Center
Langley Station, Hampton, Va.

NATIONAL AERONAUTICS AND SPACE ADMINISTRATION
WASHINGTON

November 1962

NATIONAL AERONAUTICS AND SPACE ADMINISTRATION

TECHNICAL NOTE D-1513

BUCKLING OF RING-STIFFENED CYLINDERS UNDER A PURE BENDING MOMENT AND A NONUNIFORM TEMPERATURE DISTRIBUTION

By Melvin S. Anderson and Michael F. Card

SUMMARY

Thirteen stainless-steel ring-stiffened cylinders were subjected to a pure bending load and heated rapidly until buckling occurred. For most of the cylinders the heating was not uniform around the circumference so that appreciable axial thermal stresses were present. Elementary thermal stress theory was found to be inadequate for the prediction of these thermal stresses, but a method was developed that would give satisfactory thermal stress results. By properly accounting for the thermal stress, the buckling load could be correlated with a theory for the buckling of an axially compressed ring-stiffened cylinder that is uniformly heated.

INTRODUCTION

A ring-stiffened cylinder used as a structural component in a missile or launch vehicle may undergo aerodynamic heating which, in general, is not uniform around the circumference or along the length. The resulting temperature variation causes axial thermal stresses, and the presence of cooler rings causes circumferential thermal stresses in the vicinity of the rings. These thermal stresses can cause reductions in the load carrying ability of the cylinder. The reduction of the axial compressive buckling load due to circumferential thermal stresses resulting from uniform heating is treated in reference 1, where a comparison of theoretical results and experimental data is also given. If the cylinder is heated nonuniformly around the circumference, varying axial thermal stresses as well as circumferential thermal stresses are present. References 2 and 3 present a theoretical analysis of the buckling behavior of a cylinder under a varying axial stress distribution. The results indicate that, theoretically, the maximum axial compressive stress at buckling is essentially the classical buckling stress for uniform compression.

In order to determine the effect on buckling of combinations of axial and circumferential thermal stresses and load-induced stresses, an experimental investigation was conducted and the results are reported in this paper. Ring-stiffened cylinders were loaded by a pure bending moment and then heated nonuniformly until buckling occurred. An analysis of the axial thermal stress present in the cylinder is given in the appendix. The results of this analysis in

combination with the theory of reference 1 is shown to give satisfactory correlation with the load-induced stress at cylinder buckling.

SYMBOLS

$A = \frac{Et'R^6}{E'IL^3}$

a_{in}, b_{in} Fourier coefficients in expansion of shear flow in bay i

$B = \frac{Et'R^2}{GtL^2}$

c_{in}, d_{in} Fourier coefficients defined by equations (A4)

E Young's modulus of sheet material

E' Young's modulus of ring material

G shear modulus of sheet material

I moment of inertia of ring

i index for bay or ring

L length of cylinder between rings

m number of last bay in cylinder where first bay is zero (m + 1 bays in a cylinder)

n general number of Fourier coefficient

q shear flow

R radius of cylinder

T temperature

T_{max} maximum cylinder temperature

$\overline{T}$ temperature expressed as a function of ϕ only and obtained by averaging temperature along bay length for a given value of ϕ

ΔT change in T from initial or room-temperature value

$\overline{\Delta T}$ change in $\overline{T}$ from initial or room-temperature value

$\overline{\Delta T'}$ average temperature rise of ring

t skin thickness

t' skin thickness that is effective in carrying axial loads

u axial displacement

u_{in}, u'_{in} Fourier coefficients in expansion of u_i

x axial coordinate

α coefficient of linear thermal expansion

$$\gamma = \frac{1}{n^2\left(n^2 - 1\right)^2}$$

ν, λ, μ constants defined by equations (A12), (A17), and (A20), respectively

σ general notation for axial stress

σ_x maximum axial compressive stress due to applied bending moment

σ_T thermal stress

$\sigma_{in}, \sigma'_{in}$ Fourier coefficients in expansion of σ_i

ϕ circumferential coordinate

TEST SPECIMENS

The test specimens consisted of thirteen 19-inch-diameter cylinders having a nominal wall thickness of 0.030 inch with a resultant value of R/t of approximately 300. All cylinders were of the same overall size with a total length of $45\frac{3}{4}$ inches but there were two different ring spacings. Ten specimens had nine rings and three specimens had five rings with a resultant value of L/R of 1/2 and 1, respectively. The cylinders were fabricated by spotwelding. Because of limited sheet width it was necessary to have three longitudinal splices. Fabrication details of the specimens are shown in figure 1, and the ring spacing and cylinder wall thickness for each specimen are given in table I.

The wall material was extra hard type 301 stainless steel and the Z-section rings were spun from type 304 stainless steel. The wall material was chosen so

that the variation of Young's modulus with temperature would be small and the expected stress levels would be well within the elastic range of the material. The results then would not be a function of wide changes in material properties.

TEST PROCEDURE

Rapid Heating Tests

A general view of the test setup and a detailed view of the heater installation are shown in figure 2. One end of the cylinder is supported by a heavy backstop; a pure bending load is applied at the other end by a weight cage acting through a loading frame with pin-connected linkages. Rollers between the frame and support allowed lateral and longitudinal movement which minimized any extraneous loads. The tip fixture was counterbalanced to eliminate any shear force on the cylinder.

The cylinders were heated rapidly by a 25-inch-long quartz lamp heater. For most of the tests the heater extended over approximately one-third of the circumference and was symmetrically located about the bottom extreme compression fiber of the cylinders, as shown in figure 2(b). In a few tests the heater extended around the entire cylinder in order to produce uniform heating around the circumference.

The procedure for each rapid heating test was to apply a bending moment less than the room-temperature bending strength and then heat the cylinder at a rate of approximately 20° F/sec until buckling occurred. During each test temperatures at several ring and skin locations were recorded, and in some tests strains were measured with resistance-type strain gages. The vertical deflection of the tip fixture was continuously recorded in order to identify the instant of buckling. By varying the applied load in different tests, a buckling interaction curve for load-induced stress and temperature was obtained.

Conventional room-temperature wire or foil gages were successfully used in regions where temperature did not exceed 175° F. The gage response due to temperature alone was not large compared with the overall strains being measured; therefore, the strains determined from these gages by using an appropriate temperature-response calibration curve were believed to be reasonably accurate. An attempt was made to measure strains in the heated portions of the cylinder with high-temperature strain gages. However, the gage response due to temperature was large compared with the strains being measured in the temperature range of interest. The data obtained from the high-temperature strain gages were inconsistent and generally could not be used as an accurate measure of strain in the cylinder.

Room-Temperature Tests

A limited number of tests conducted at room temperature were made in order to get an idea of the scatter to be expected in the data and to determine the

reduction from the classical buckling stress for cylinders of the material and construction that were used. The room-temperature bending strength was determined for two cylinders having $\frac{L}{R} = \frac{1}{2}$ and one cylinder having $\frac{L}{R} = 1$. Test procedure was similar to that indicated for the rapid heating tests except load was applied in the absence of heating by means of a hydraulic jack instead of the weight cage.

RESULTS AND DISCUSSION

Buckling

The results of the investigation are given in table I and are plotted in figure 3. For each specimen the maximum load-induced compressive stress is plotted as a function of the maximum cylinder temperature at time of buckling. The maximum cylinder temperature was taken as the temperature at the bottom or extreme compressive fiber of the cylinder and midway between rings in the bay nearest to the middle of the cylinder. This temperature was the actual maximum or nearly the maximum for all cylinders tested.

It is of interest to compare the results at room temperature with predictions based on experimental cylinder buckling coefficients which are available from tests on aluminum cylinders (ref. 4). It can be seen in figure 3 that the experimental room-temperature buckling data for the steel cylinders indicate a buckling coefficient less than the average but greater than the lower limit of the data on aluminum cylinders. There are not enough test data to establish whether any real difference in cylinder buckling coefficient exists for the two materials; however, any difference is probably small.

If a cylinder were heated slowly and uniformly around the circumference so as to produce no thermal stress, the cylinder buckling stress would be reduced in proportion to the reduction in E. The amount of this reduction is indicated by the short-dash curves in figure 3. Rapid but uniform heating causes circumferential thermal stresses in the vicinity of the cooler rings. The interaction of axial and circumferential stress results in a reduced buckling stress as shown by the circle test points in figure 3. The solid-line curve is based on the theory of reference 1 and tends to overestimate the test results somewhat. As in reference 1, it is necessary to modify the theoretical predictions based on the reduction in room-temperature cylinder buckling strength from the classical value. Inasmuch as this reduction had not been established for the type of cylinders tested, the results of the three room-temperature tests that were made were averaged and this value was used in determining the reduction in buckling stress from the classical value. The results of reference 1 are in the form of an interaction curve of axial compressive stress and the difference of the average skin and ring temperatures. In order to express the results in terms of T_{max} it is necessary to know the variation of these two average temperatures with T_{max}. This variation is given in figure 4 where the average temperature of the interior bays and rings and also the difference in these temperatures are plotted as a function of T_{max}. The variation of α and E with temperature, which is also necessary for the calculations, is given in figure 5.

For nonuniform heating, the load-induced stress at buckling is further reduced as evidenced by the square test points in figure 3. For this condition axial thermal stresses are present which might be expected to add directly to the load-induced stress so that buckling would occur when the total compressive stress (load-induced stress plus axial thermal stress) is equal to the buckling stress for uniform heating, as calculated from reference 1. Support for such an assumption is given in references 2 and 3, where buckling of a cylinder under varying axial compressive stress is shown to be relatively insensitive to the stress distribution but dependent on the maximum value of the compressive stress. When the load-induced stress at buckling is estimated by subtracting the axial thermal stress from the buckling stress for uniform rapid heating as calculated from reference 1, the long-short-dash curves in figure 3 result. Reasonable agreement is obtained except at the highest stress level where the results are somewhat unconservative for both the uniform and nonuniform heating tests. In the test of cylinder 6, failure occurred almost immediately after the heating started and the buckling temperature was much lower than was expected on the basis of results from the other tests. The values of the load-induced stress and buckling temperature were rechecked and no discrepancies were found. Therefore, a similar test was made on cylinder 7; this result was in agreement with the trend established by the other data.

Calculation of thermal stress in cylinders involves more than the elementary thermal-stress computation, in which plane sections are assumed to remain plane, even if the internal region of the cylinder has a temperature distribution independent of length over many bays. The common practice, which applies to solid-section beams, of assuming that the effect of ends can be neglected at distances from the ends of the order of the beam depth is not a good assumption for cylindrical shells. A method of calculating cylinder thermal stresses for a general temperature distribution is given in the appendix. This method was used in determining the long-short-dash curve in figure 3. A detailed discussion of the thermal stress present in the test cylinders is given in the next section.

The behavior of the specimens at buckling was typical of cylinders loaded in pure bending. Diamond-shaped buckles which extended to the vicinity of the neutral axis snapped in suddenly at the buckling temperature. Figure 6 is a photograph of cylinder 9 after buckling had occurred.

Temperature and Thermal Stress Distribution

A typical experimental temperature distribution along the bottom or most severely heated portion of the cylinder is indicated in figure 7 for a cylinder with $\frac{L}{R} = \frac{1}{2}$. The curves shown were faired through a number of data points. Temperatures were essentially symmetric about the center line and this symmetry was used in all calculations. Note the heat-sink effect of the rings and that the four interior bays received approximately equal heating. For the cylinders with $\frac{L}{R} = 1$ the temperature distribution was essentially that which would be obtained from figure 7 by removing the heat-sink effect at the even-numbered ring stations.

In the circumferential direction, temperature variations as shown in figure 8 occurred midway between rings for cylinders heated on one side only. The curves shown are an analytical approximation of the data which was used in some of the thermal-stress calculations.

The axial thermal stresses in the cylinders tested were calculated by using the analysis given in the appendix. A comparison between theoretical and experimental thermal stresses is shown in figure 9 where both longitudinal and circumferential thermal stress distributions are shown. The thermal stress is of most interest at the bottom ($\phi = 0$) of the cylinder where the temperature is the greatest and where the load-induced compressive stress is a maximum. The bottom of the cylinder is the region assumed critical for buckling even though, as shown in the lower portion of figure 9(b), it is not the region of maximum compressive thermal stress. The compressive thermal stress is somewhat greater 20° away from the bottom because of the essentially constant temperature over a considerable portion of the cylinder circumference. However, the sum of the load-induced stress and thermal stress is a maximum at the bottom of the cylinder for most of the tests. At the higher temperatures the stress at the bottom of the cylinder is slightly less than the maximum stress. Nevertheless, the bottom is still probably the most critical region for buckling because the circumferential thermal stress which is also involved in the buckling is a maximum at the bottom of the cylinder and decays to zero in the unheated portion of the cylinder.

As mentioned previously, accurate values of experimental thermal stress were not obtained over portions of the cylinder heated directly by the lamps. However, the comparison of measured and calculated stresses for the cooler areas does give an indication of the expected accuracy in calculating the thermal stress in the heated areas which are critical for buckling. In general, agreement between experiment and theory is good except that results of the calculations are greater than experiment in certain areas. The dashed curves in figure 9(a) correspond to the elementary thermal stress in each bay and are seen to be considerably different from either the experimental or theoretical thermal stresses.

One factor which was not accounted for in the theory was the effect of splices which are located at $\phi = \pm 67\frac{1}{2}^\circ$ and $\phi = 180^\circ$. Along the splice at $\phi = 180^\circ$ which was the top of the cylinder and not in the region critical for buckling, the magnitude of the experimental stresses was, for the most part, less than that of the calculated stresses. Another factor which was not accounted for was the variation in the quantity αE. Above 600° F, αE decreases with temperature so that the calculated thermal stresses are probably too high in this temperature range. The comparison of calculated and experimental buckling stresses (fig. 3(a)) also indicates that the theoretical thermal stresses are greater than the actual thermal stresses at the higher temperatures.

CONCLUDING REMARKS

The results of bending tests of rapidly heated, ring-stiffened stainless-steel cylinders have been presented. A few tests were made at room temperature and the experimental buckling coefficients were found to be essentially the same

or only slightly less than those which have been obtained for aluminum cylinders. The test results for uniform heating around the circumference could be correlated satisfactorily with a theory for the interaction of axial compressive stresses and circumferential thermal stresses. When the heating was nonuniform, substantial axial thermal stresses were present. These stresses, which were considerably different from those predicted by elementary theory, showed reasonable agreement with a theory that takes into account radial deflections of the skin and rings. The load-induced stress at buckling for the nonuniform heating tests could be satisfactorily predicted by subtracting the calculated axial thermal stress from the predicted buckling stress for uniform rapid heating.

Langley Research Center,
National Aeronautics and Space Administration,
Langley Station, Hampton, Va., August 29, 1962.

APPENDIX

AXIAL THERMAL STRESS IN A RING-STIFFENED CYLINDER WITH AN ARBITRARY TEMPERATURE DISTRIBUTION

The elementary theory of thermal stress can be used satisfactorily for solid-section beams if the interior portion has a temperature distribution essentially independent of length. In the vicinity of a free end the thermal stress must decay to zero. However, this condition usually is of little concern because only the maximum thermal stress which occurs away from the ends and which can be calculated by elementary theory is generally required. The elementary theory, when applied to a ring-stiffened cylinder, does not account for radial deflections of the rings or cylinder wall. Inasmuch as the dimensions of most ring-stiffened cylinders are such that these deflections cannot be ignored without introducing appreciable inaccuracies in analytical results, the elementary theory must be modified so as to satisfy continuity between rings and sheet as well as the equations of statics. The following development yields self-equilibrating stress distributions which can be superimposed on the elementary thermal stress distribution so as to maintain the continuity of the cylinder. The method is essentially the same as that of reference 5 where self-equilibrating stress distributions were found that could be superimposed on the stresses obtained from the elementary theory of torsion and bending to yield the correct stress distribution for a cylinder subjected to lateral loads.

General Theory

For purposes of analysis the cylinder is divided into bays small enough that the temperature in each bay is a function of ϕ only or

$$T_i = \overline{T}_i(\phi) \tag{A1}$$

where i denotes the bay number of the cylinder which has a total of $m + 1$ bays. The bay notation and coordinate system are shown in figure 10. The bar in $\overline{T}_i(\phi)$ denotes that at a given value of ϕ an average temperature over the bay length is used. The most satisfactory arrangement is obtained when the ring spacing is small enough that equation (A1) is a reasonable approximation of the temperature for bay widths equal to the ring spacing. If the temperature variation in the axial direction is too large between rings, several bays may be required between rings. In this case the bays between the actual rings are assumed to be separated by a fictitious ring having a moment of inertia based on the effective sheet material in each bay. With this assumption it is seen that the bay length and ring spacing are not necessarily equal.

The thermal stress in the cylinder may be obtained by a process similar to that used in elementary thermal stress problems. If each bay is rigidly constrained, the resulting stress distribution is given by

$$\sigma_i = -\alpha_i E_i \overline{\Delta T}_i(\phi) \tag{A2}$$

In each bay this stress system is independent of x_i, but for equilibrium the constraints at the end of each bay are loaded by forces with intensity $\sigma_i t'_i$ where σ_i is given by equation (A2). If a loading intensity of $-\sigma_i t'_i$ is applied to the cylinder at the ends of each bay, the forces on the constraints are removed. Therefore, the constraints are no longer needed to maintain the cylinder in equilibrium. Thus, the thermal stress is calculated by adding the stress given in equation (A2) to the stress system obtained from loading the cylinder at the end of each bay with stresses equal but of opposite sign to those given in equation (A2).

Solution of stress-distribution problem.- In solving this stress-distribution problem it is convenient to express the applied stresses at the end of each bay as a Fourier series

$$\alpha_i E_i \overline{\Delta T}_i = \sum_{n=0}^{\infty} \left(c_{in} \cos n\phi + d_{in} \sin n\phi \right) \tag{A3}$$

The Fourier coefficients c_{in} and d_{in} may be determined as

$$\left.\begin{aligned} c_{i0} &= \frac{1}{2\pi} \int_0^{2\pi} \alpha_i E_i \overline{\Delta T}_i \, d\phi \\ c_{in} &= \frac{1}{\pi} \int_0^{2\pi} \alpha_i E_i \overline{\Delta T}_i \cos n\phi \, d\phi \\ d_{in} &= \frac{1}{\pi} \int_0^{2\pi} \alpha_i E_i \overline{\Delta T}_i \sin n\phi \, d\phi \end{aligned}\right\} \tag{A4}$$

The stress distributions corresponding to c_{i0}, c_{i1}, and d_{i1} are a uniform axial stress distribution and two bending-moment distributions about two perpendicular axes. These stresses do not vary with x_i and are seen to yield the elementary thermal stress solution for bay i when added to equation (A2). The remaining terms ($n > 1$) represent a self-equilibrating stress distribution which decays with increasing distance away from bay i.

The solution of the stress-distribution problem for $n > 1$ can be obtained by an extension of the method presented in reference 5. In the theory of reference 5 it is assumed that the strain in the circumferential direction is zero. All material which resists axial stresses (including longitudinal stringer material) is represented by an effective thickness t'_i, whereas the actual thickness t is assumed to resist only shear stresses. By using these

assumptions, the self-equilibrating shear flow and direct stress in bay i and the associated axial displacements can be written as follows (see ref. 5):

$$q_i(\phi) = \sum_{n=2}^{\infty} \left(a_{in} \sin n\phi + b_{in} \cos n\phi \right) \tag{A5}$$

$$\sigma_i(x_i,\phi) = \sum_{n=2}^{\infty} \left[\sigma_{in}(x_i) \cos n\phi + \sigma'_{in}(x_i) \sin n\phi \right] \tag{A6}$$

$$u_i(x_i,\phi) = \sum_{n=2}^{\infty} \left[u_{in}(x_i) \cos n\phi + u'_{in}(x_i) \sin n\phi \right] \tag{A7}$$

where

$$\left.\begin{aligned} \sigma_{in}(x_i) &= -\frac{nx_i}{Rt'_i} a_{in} + \sigma_{in}(0) \\ \sigma'_{in}(x_i) &= \frac{nx_i}{Rt'_i} b_{in} + \sigma'_{in}(0) \end{aligned}\right\} \tag{A8}$$

and

$$\left.\begin{aligned} u_{in}(x_i) &= -\frac{nx_i^2}{2E_iRt'_i} a_{in} + \frac{\sigma_{in}(0)}{E_i} x_i + u_{in}(0) \\ u'_{in}(x_i) &= \frac{nx_i^2}{2E_iRt'_i} b_{in} + \frac{\sigma'_{in}(0)}{E_i} x_i + u'_{in}(0) \end{aligned}\right\} \tag{A9}$$

The complete stress distribution can be obtained once the Fourier coefficients a_{in} and b_{in} are determined. The solution for a_{in} and b_{in} for the problem considered herein is the same as that in reference 5 except that the equations for equilibrium of forces at a ring (see fig. 10) are changed as follows:

$$\left.\begin{aligned} \left[\sigma_{i-1,n}(L_{i-1}) - c_{i-1,n}\right] t'_{i-1} &= \left[\sigma_{in}(0) - c_{in}\right] t'_i \\ \left[\sigma'_{i-1,n}(L_{i-1}) - d_{i-1,n}\right] t'_{i-1} &= \left[\sigma'_{in}(0) - d_{in}\right] t'_i \end{aligned}\right\} \tag{A10}$$

In reference 5 the thicknesses t'_i are omitted in error and there are no applied in-plane stresses so that c_{in} and d_{in} do not appear.

From equation (A3) it can be seen that the coefficients c_{in} correspond to symmetrical loadings and the coefficients d_{in} correspond to antisymmetrical loadings. Since the solution for either loading is essentially the same, only the solution for the symmetrical terms, corresponding to the heating condition for the cylinders reported herein, are considered in the following development. A recurrence formula for the symmetrical shear-flow coefficients a_{in} is obtained as in reference 5 in the form

$$a_{i-2,n}\left(\frac{\nu_1}{E'_{i-1}I_{i-1}}\right) - a_{i-1,n}\left[\frac{\nu_1}{E'_{i-1}I_{i-1}}\left(1 + \frac{E'_{i-1}I_{i-1}}{E'_iI_i} + \frac{6B_{i-1} - n^2}{6A_{i-1}\gamma}\right) + \frac{\nu_2}{E'_iI_i}\right]$$

$$+ a_{in}\left[\frac{\nu_1}{E'_iI_i} + \frac{\nu_2}{E'_iI_i}\left(1 + \frac{E'_iI_i}{E'_{i+1}I_{i+1}} + \frac{6B_i - n^2}{6A_i\gamma}\right) + \frac{\nu_3}{E'_{i+1}I_{i+1}} + \frac{\nu_4 n^2}{2E'_iI_iA_i\gamma}\right]$$

$$- a_{i+1,n}\left[\frac{\nu_2}{E'_{i+1}I_{i+1}} + \frac{\nu_3}{E'_{i+1}I_{i+1}}\left(1 + \frac{E'_{i+1}I_{i+1}}{E'_{i+2}I_{i+2}} + \frac{6B_{i+1} - n^2}{6A_{i+1}\gamma}\right)\right] + a_{i+2,n}\left(\frac{\nu_3}{E'_{i+2}I_{i+2}}\right)$$

$$= \frac{n}{2R^5\gamma}\left[\frac{\nu_1 L_{i-1}^2}{E_{i-1}t'_{i-1}}\left(c_{in}t'_{in} - c_{i-1,n}t'_{i-1,n}\right) + \frac{\nu_3 L_{i+1}^2}{E_{i+1}t'_{i+1}}\left(c_{i+1}t'_{i+1} - c_{in}t'_i\right)\right] \qquad \text{(A11)}$$

$$(2 \leqq i \leqq m - 2)$$

where

$$\left.\begin{aligned}
\nu_1 &= \frac{1}{L_{i-1}^2}\left(\frac{E_it'_iL_{i-1}}{E_{i-1}t'_{i-1}L_i} + \frac{L_{i-1}}{L_{i+1}}\right) \\
\nu_2 &= \frac{1}{L_i^2}\left(\frac{2L_i}{L_{i+1}} + \frac{E_it'_iL_{i-1}}{E_{i-1}t'_{i-1}L_{i+1}} + \frac{E_it'_i}{E_{i+1}t'_{i+1}}\right) \\
\nu_3 &= \frac{1}{L_{i+1}^2}\left(\frac{E_it'_iL_{i-1}}{E_{i-1}t'_{i-1}L_i} + 1\right) \\
\nu_4 &= \frac{1}{L_i^2}\left(\frac{L_i}{L_{i+1}} + \frac{E_it'_iL_{i-1}}{E_{i-1}t'_{i-1}L_{i+1}} + \frac{E_i^2t'^2_iL_{i-1}}{E_{i-1}E_{i+1}t'_{i-1}t'_{i+1}L_i} + \frac{E_it'_i}{E_{i+1}t'_{i+1}}\right)
\end{aligned}\right\} \qquad \text{(A12)}$$

and

$$\left.\begin{aligned} \gamma &= \frac{1}{n^2\left(n^2-1\right)^2} \\ A_i &= \frac{E_i t'_i R^6}{E'_i I_i L_i^3} \\ B_i &= \frac{E_i t'_i R^2}{G_i t_i L_i^2} \end{aligned}\right\} \tag{A13}$$

Boundary conditions.- Equation (A11) applies to any interior bay i when there are at least two adjacent bays on both sides of the given bay. This condition is not satisfied at the ends of the cylinder and special equations are necessary which are determined by the boundary conditions. In all cases one boundary condition is that the radial deflection of the cylinder wall is equal to the radial deflection of the ring at the end of the cylinder. When there is no axial stress on the end cross section, which is sometimes referred to as a free end, an additional boundary condition is

$$\sigma_{0n}(0) - c_{0n} = 0 \tag{A14}$$

The following equations are obtained as a result of these boundary conditions:

$$\begin{aligned} &a_{0n}\left[\frac{\lambda_1}{E'_0 I_0}\left(1 + \frac{E'_0 I_0}{E'_1 I_1} + \frac{6B_0 - n^2}{6A_0\gamma}\right) + \frac{\lambda_2}{E'_1 I_1} + \frac{\lambda_3 n^2}{2E'_0 I_0 A_0 \gamma}\right] \\ &- a_{1n}\left[\frac{\lambda_2}{E'_1 I_1}\left(1 + \frac{E'_1 I_1}{E'_2 I_2} + \frac{6B_1 - n^2}{6A_1\gamma}\right) + \frac{\lambda_1}{E'_1 I_1}\right] + a_{2n}\left(\frac{\lambda_2}{E'_2 I_2}\right) \\ &= \frac{n}{2R^5\gamma}\left(\frac{\lambda_1 L_0^2 c_{0n}}{E_0} + \frac{\lambda_2 L_1^2 c_{1n}}{E_1}\right) \end{aligned} \tag{A15}$$

and

$$\begin{aligned} &-a_{0n}\left(\frac{\lambda_2}{E'_1 I_1} - \frac{\lambda_5 n^2}{2E'_0 I_0 A_0 \gamma}\right) + a_{1n}\left[\frac{\lambda_2}{E'_1 I_1}\left(1 + \frac{E'_1 I_1}{E'_2 I_2} + \frac{6B_1 - n^2}{6A_1\gamma}\right) + \frac{\lambda_4}{E'_2 I_2}\right. \\ &\left. + \frac{\lambda_6 n^2}{2E'_1 I_1 A_1 \gamma}\right] - a_{2n}\left[\frac{\lambda_2}{E'_2 I_2} + \frac{\lambda_4}{E'_2 I_2}\left(1 + \frac{E'_2 I_2}{E'_3 I_3} + \frac{6B_2 - n^2}{6A_2\gamma}\right)\right] + a_{3n}\left(\frac{\lambda_4}{E'_3 I_3}\right) \\ &= \frac{n}{2R^5\gamma}\left[\frac{c_{1n}}{E_1} + \frac{\lambda_4 L_2^2}{E_2 t'_2}\left(c_{2n} t'_2 - c_{1n} t'_1\right)\right] \end{aligned} \tag{A16}$$

where

$$\left.\begin{aligned}
\lambda_1 &= \frac{1}{L_0 L_1} \\
\lambda_2 &= \frac{1}{L_1^2} \\
\lambda_3 &= \frac{1}{L_0^2}\left(\frac{L_0}{L_1} + \frac{E_0 t'_0}{E_1 t'_1}\right) \\
\lambda_4 &= \frac{1}{L_1 L_2} \\
\lambda_5 &= \frac{1}{L_0^2}\left(\frac{E_0 t'_0 L_2}{E_2 t'_2 L_1} + \frac{E_0 t'_0}{E_1 t'_1}\right) \\
\lambda_6 &= \frac{1}{L_1^2}\left(\frac{E_1 t'_1 L_2}{E_2 t'_2 L_1} + 1\right)
\end{aligned}\right\} \qquad (A17)$$

If the end of bay zero is clamped, the axial displacements due to an axial force and a bending moment may be allowed, but the displacements due to the self-equilibrating force system are constrained so that $u_0(0,\phi)$ is equal to zero which implies $u_{0n}(0)$ is equal to zero. The following equations are obtained for a clamped end:

$$a_{0n}\left[\frac{\mu_1}{E'_1 I_1} + \frac{\mu_2}{E'_0 I_0}\left(1 + \frac{E'_0 I_0}{E'_1 I_1} + \frac{6B_0 - n^2}{6A_0\gamma}\right) + \frac{\mu_3 n^2}{2E'_0 I_0 A_0 \gamma}\right]$$
$$- a_{1n}\left[\frac{\mu_1}{E'_1 I_1}\left(1 + \frac{E'_1 I_1}{E'_2 I_2} + \frac{6B_1 - n^2}{6A_1\gamma}\right) + \frac{\mu_2}{E'_1 I_1}\right] + a_{2n}\left(\frac{\mu_1}{E'_2 I_2}\right)$$
$$= \frac{n}{2R^5\gamma}\,\frac{c_{1n}t'_1 - c_{0n}t'_0}{E_1 t'_1} \qquad (A18)$$

and

$$-a_{0n}\left[\frac{\mu_5}{E'_1 I_1} + \frac{\mu_6}{E'_0 I_0}\left(1 + \frac{E'_0 I_0}{E'_1 I_1} + \frac{6B_0 - n^2}{6A_0\gamma}\right)\right] + a_{1n}\left[\frac{\mu_4}{E'_2 I_2}\right.$$
$$\left. + \frac{\mu_5}{E'_1 I_1}\left(1 + \frac{E'_1 I_1}{E'_2 I_2} + \frac{6B_1 - n^2}{6A_1\gamma}\right) + \frac{\mu_6}{E'_1 I_1} + \frac{\mu_7 n^2}{2E'_1 I_1 A_1 \gamma}\right]$$
$$- a_{2n}\left[\frac{\mu_4}{E'_2 I_2}\left(1 + \frac{E'_2 I_2}{E'_3 I_3} + \frac{6B_2 - n^2}{6A_2\gamma}\right) + \frac{\mu_5}{E'_2 I_2}\right] + a_{3n}\left(\frac{\mu_4}{E'_3 I_3}\right)$$
$$= \frac{n}{2R^5\gamma}\left[\frac{\mu_6 L_0^2}{E_0 t'_0}\left(c_{1n}t'_1 - c_{0n}t'_0\right) + \frac{\mu_4 L_2^2}{E_2 t'_2}\left(c_{2n}t'_2 - c_{1n}t'_1\right)\right] \qquad (A19)$$

where

$$\left.\begin{aligned}
\mu_1 &= \frac{1}{L_1^2} = \lambda_2 \\
\mu_2 &= \frac{1}{L_0^2}\left(\frac{2L_0}{L_1} + \frac{E_0 t'_0}{E_1 t'_1}\right) \\
\mu_3 &= \frac{1}{L_0^2}\left(\frac{E_0 t'_0}{E_1 t'_1} + \frac{L_0}{L_1}\right) = \lambda_3 \\
\mu_4 &= \frac{1}{L_2^2}\left(\frac{E_0 t'_0 L_2}{E_1 t'_1 L_0} + \frac{L_2}{L_1}\right) \\
\mu_5 &= \frac{1}{L_1^2}\left(\frac{2E_0 t'_0 L_1}{E_1 t'_1 L_0} + \frac{E_0 t'_0 L_2}{E_2 t'_2 L_0} + 1\right) \\
\mu_6 &= \frac{1}{L_0^2}\left(\frac{E_0 t'_0 L_2}{E_2 t'_2 L_1} + \frac{E_0 t'_0}{E_1 t'_1}\right) = \lambda_5 \\
\mu_7 &= \frac{1}{L_1^2}\left(\frac{E_1 t'_0 L_2}{E_2 t'_2 L_0} + \frac{E_1 t'_1 L_2}{E_2 t'_2 L_1} + \frac{E_0 t'_0 L_2}{E_2 t'_2 L_0} + 1\right)
\end{aligned}\right\} \qquad (A20)$$

The notation used in equations (A11) to (A20) is essentially that of reference 5 except for the presence of a different Young's modulus for each bay and ring. Boundary conditions for the opposite end of the cylinder, which is denoted by bay m, may be obtained from equations (A15) to (A20) by a suitable change of subscripts. The subscripts which refer to bay numbers 0, 1, and 2 are replaced with the subscripts m, $m - 1$, and $m - 2$, respectively. Subscripts 0, 1, 2, and 3 which refer to ring numbers and occur in the term $E'_i I_i$ are replaced by $m + 1$, m, $m - 1$, and $m - 2$, respectively. It is also necessary to change the algebraic sign of the right-hand side of equations (A15), (A16), (A18), and (A19). The condition of zero radial deflection of the cylinder wall at the ends can be specified by allowing the appropriate ring moment of inertia (I_0 or I_{m+1}) to approach infinity. For the limiting case of rigid rings where all moments of inertia I_i approach infinity, the governing equations are greatly simplified.

The application of equation (A11) and the appropriate boundary conditions results in $m + 1$ equations for the determination of the $m + 1$ different values of a_{in}. If the stress at the end of a cylinder is specified as zero, the axial stress distribution can be determined from the coefficients a_{in} and

the use of equations (A8) and (A10). If the axial displacement is specified as zero at the ends, the axial stress distribution is determined from the coefficients a_{in} and equations (A8) to (A10). Solutions for unsymmetrical loadings can be obtained by replacing a_{in} with $-b_{in}$ in equations (A11), (A15), (A16), (A18), and (A19).

The axial thermal stress at any ring can now be written for the general case as

$$\sigma_{Ti}(0) = -\alpha_i E_i \overline{\Delta T}_i + c_{i0} + c_{i1} \cos \phi + d_{i1} \sin \phi + \sum_{n=2}^{\infty} \left[\sigma_{in}(0)\cos n\phi + \sigma'_{in}(0)\sin n\phi\right] \quad \text{(A21)}$$

There is a linear variation of σ_{Ti} between each ring. Note that the first four terms on the right-hand side of equation (A21) represent the elementary thermal-stress solution for each bay.

Application of Equations to Test Cylinders

The equations presented thus far are very general in that each bay length and ring size may be different. Also material properties may be different for each bay and ring. However, the material properties are assumed to be constant around the circumference for a given ring or bay; this means some average or effective value of E must be assigned to each ring and bay if there is a circumferential variation in E. The manner in which E appears in the recurrence formula and boundary conditions is in the ratio of E for the material in one bay or ring to E for the material in a nearby bay or ring. These equations involve, at the most, five adjacent cylinder bays; if E does not vary greatly within these bays, the ratio of the values of E for different bays may be assumed to be unity. With this assumption the actual (or effective) value of E is not required for the solution of equations (A11), (A15), (A16), (A18), and (A19). This assumption is made in the calculations for the test cylinder of this report. The calculation of c_{in} and d_{in} also involves E but only in the product αE which tends to be more constant with temperature than either α or E. A constant value of 0.24 ksi/$^{\circ}$F was assumed in all calculations.

The axial thermal stress for the test cylinders may be determined by the following procedure. A schematic diagram of a typical test cylinder is shown in figure 11 which also includes the dimensions and ring moments of inertia necessary for the calculation. All cylinders were of the same overall size but there were two values of ring spacing. The idealization shown in figure 11 has equal bay lengths corresponding to $\frac{L}{R} = \frac{1}{2}$. For $\frac{L}{R} = 1$ the same bay length is used but the even-numbered ring locations, which correspond to midway between rings in the actual cylinder, are assigned a moment of inertia equal to that of the wall material one bay wide. The end bays are actually shorter than the other

bays and terminate at a 3/16-inch adapter ring which is fastened to a very heavy attachment ring. (See fig. 1.) The whole assembly is then bolted on one end to a very stiff tip fixture and on the other end to a backstop. Because of this stiff end attachment, the end bays were assumed to be clamped and to have a length equal to that of the other bays. The heating is assumed symmetrical about $\phi = 0$; therefore, only the equations involving a_{in} are needed. Because of symmetry about ring 5, $a_{5n} = -a_{4n}$, $a_{6n} = -a_{3n}$, and $c_{5n} = c_{4n}$; thus, equations for only five bays have to be considered. With these assumptions and boundary condition, the equations determining a_{in} can be obtained from equations (A11), (A18), and (A19) in a simplified form as follows:

$$\left.\begin{aligned}
&a_{0n}\left(24A_1\gamma + 18B + 3n^2\right) - a_{1n}\left(24A_1\gamma + 6A_2\gamma + 6B - n^2\right) + a_{2n}\left(6A_2\gamma\right) = \frac{3Rt'n}{L}\left(c_{1n} - c_{0n}\right)\\
&-a_{0n}\left(18A_1\gamma + 6B - n^2\right) + a_{1n}\left(18A_1\gamma + 18A_2\gamma + 12B + 4n^2\right)\\
&- a_{2n}\left(6A_1\gamma + 18A_2\gamma + 6B - n^2\right) + a_{3n}\left(6A_1\gamma\right)\\
&= \frac{3Rt'n}{L}\left(c_{2n} - c_{0n}\right)\\
&a_{0n}\left(6A_1\gamma\right) - a_{1n}\left(6A_1\gamma + 18A_2\gamma + 6B - n^2\right) + a_{2n}\left(18A_1\gamma + 18A_2\gamma + 12B + 4n^2\right)\\
&- a_{3n}\left(18A_1\gamma + 6A_2\gamma + 6B - n^2\right) + a_{4n}\left(6A_2\gamma\right)\\
&= \frac{3Rt'n}{L}\left(c_{3n} - c_{1n}\right)\\
&a_{1n}\left(6A_2\gamma\right) - a_{2n}\left(18A_1\gamma + 6A_2\gamma + 6B - n^2\right) + a_{3n}\left(18A_1\gamma + 18A_2\gamma + 12B + 4n^2\right)\\
&- a_{4n}\left(12A_1\gamma + 18A_2\gamma + 6B - n^2\right)\\
&= \frac{3Rt'n}{L}\left(c_{4n} - c_{2n}\right)\\
&a_{2n}\left(6A_1\gamma\right) - a_{3n}\left(6A_1\gamma + 24A_2\gamma + 6B - n^2\right) + a_{4n}\left(36A_1\gamma + 24A_2\gamma + 18B + 3n^2\right)\\
&= \frac{3Rt'n}{L}\left(c_{4n} - c_{3n}\right)
\end{aligned}\right\} \qquad (A22)$$

In equations (A22) the subscripts on L, B, and t' have been dropped inasmuch as there is no change in these quantities with bay number. For cylinders with $\frac{L}{R} = 1$ there are two independent values of A_i given by A_1 and A_2.

The calculation of the coefficients c_{in} by use of equations (A4) requires some special consideration. The final determination of the thermal stress often involves small differences of large numbers. An error of less than 1 percent in determining c_{in} in some instances can easily cause errors greater than 10 percent in thermal stress. Thus, it is especially important to obtain an accurate consistent set of values for c_{in}. Graphical or numerical integration of equations (A4), unless done very accurately, may lead to serious errors in the final result. For this reason, an analytical expression for the temperature distribution was obtained that yielded an analytical expression for c_{in}. Thus, c_{in} could be determined as accurately as necessary and all values would be consistent with each other. The expression for the temperature rise was applied to all bays and is given by

$$\left.\begin{aligned} \frac{\overline{\Delta T}_i}{\overline{\Delta T}_i(0)} &= \cos \phi + 0.05 \sin 3\phi \qquad (0^\circ \leqq \phi \leqq 60^\circ) \\ \frac{\overline{\Delta T}_i}{\overline{\Delta T}_i(0)} &= \cos \phi \qquad (60^\circ \leqq \phi \leqq 80^\circ) \\ \frac{\overline{\Delta T}_i}{\overline{\Delta T}_i(0)} &= \cos 80^\circ \, e^{-0.0623(\phi - 80^\circ)} \qquad (80^\circ \leqq \phi \leqq 180^\circ) \end{aligned}\right\} \quad \text{(A23)}$$

This temperature distribution was taken to be symmetrical about $\phi = 0$. The bars denote an average temperature rise over a bay length. This average temperature rise in a given bay was essentially a constant times the temperature rise at midbay. Thus, the expressions on the right-hand side of equations (A23) apply equally well to the ratio $\Delta T_i / \Delta T_i(0)$. The curves of figure 8 were calculated from equations (A23) by replacing $\overline{\Delta T}_i / \overline{\Delta T}_i(0)$ with $\Delta T_i / \Delta T_i(0)$, and the agreement between measured and calculated values is indicative of the accuracy of equations (A23) for both the average and midbay temperatures. Values of $\Delta T_i(0)$ and $\overline{\Delta T}_i(0)$, which are necessary to calculate the temperature distribution, were obtained for each bay from the measured temperature distributions and are given in figure 12 as a function of the maximum cylinder temperature.

After the coefficients a_{in} have been determined, $\sigma_{0n}(0)$ can be obtained from equations (A8) to (A10) with the use of the conditions $u_{0n}(0) = u_{5n}(0) = 0$:

$$\sigma_{0n}(0) = \frac{1}{5}\left[\frac{n^2}{2} \frac{L}{nRt'}\left(9a_{0n} + 7a_{1n} + 5a_{2n} + 3a_{3n} + a_{4n}\right) - \left(c_{1n} + c_{2n} + c_{3n} + c_{4n} - 4c_{0n}\right)\right] \quad \text{(A24)}$$

The remaining coefficients $\sigma_{in}(0)$ are determined from the first of equations (A8). The thermal stress in the test cylinders was calculated by using equation (A21); a comparison of the calculated and experimental thermal stresses is shown in figure 9. Terms up to $n = 10$ were used in the calculations. This number of terms resulted in suitable convergence except for the stresses in bay 2, which are estimated to deviate less than 5 percent from the value that would be obtained by taking many more terms. This behavior is believed to be caused by the steep longitudinal temperature gradient in this bay. The assumption of clamped ends is supported by the agreement of experiment and theory in the vicinity of the ends. A characteristic of cylinder behavior which is contrary to that observed in solid-section beams is the slow decay of the thermal stress away from the heated area. (See fig. 9(a).) The stress distribution is affected by ring stiffness as illustrated in figure 13 where the axial thermal stress along the bottom of the cylinder is plotted for three values of ring stiffness. The ring stiffnesses used were: completely rigid $(I_i = \infty)$, the actual stiffness as measured by the calculated ring moment of inertia, and one-half the calculated stiffness. Little difference is seen between the curves for rings of finite stiffness but the stress distribution obtained by assuming rigid rings exhibits a much greater rate of stress decay. Even though the rings used were reasonably stiff by most standards, their behavior for thermal stress was far from that of a rigid ring.

REFERENCES

1. Anderson, Melvin S.: Combinations of Temperature and Axial Compression Required for Buckling of a Ring-Stiffened Cylinder. NASA TN D-1224, 1962.

2. Seide, Paul, and Weingarten, V. I.: On the Buckling of Circular Cylindrical Shells Under Pure Bending. Trans. ASME, Ser. E - Jour. Appl. Mech., vol. 28, no. 1, Mar. 1961, pp. 112-116.

3. Abir, David, Hoff, N. J., Nardo, S. V., Pohle, Frederick V., Vafakos, William, and Wan, Koon-Sang: Thermal Buckling of Circular Cylindrical and Conical Thin-Walled Shells. WADC Tech. Rep. 58-104, ASTIA Doc. No. AD 151068, U.S. Air Force, Apr. 1958.

4. Peterson, James P.: Bending Tests of Ring-Stiffened Circular Cylinders. NACA TN 3735, 1956.

5. Duberg, John E., and Kempner, Joseph: Stress Analysis by Recurrence Formula of Reinforced Circular Cylinders Under Lateral Loads. NACA TN 1219, 1947.

TABLE I

RESULTS FOR BENDING AND HEATING TESTS OF RING-STIFFENED CYLINDERS

Cylinder	t, in.	L/R	σ_x, ksi	T_{max}, ^{o}F	Type of heating
1	0.0306	1/2	35.1	Room	None
2	.0301	1/2	38.1	Room	None
3	.0305	1	40.4	Room	None
4	.0305	1/2	29.4	380	Uniform
5	.0303	1/2	24.4	800	Uniform
6	.0306	1/2	29.4	120	Nonuniform
7	.0306	1/2	29.4	250	Nonuniform
8	.0307	1/2	24.1	450	Nonuniform
9	.0304	1/2	19.1	625	Nonuniform
10	.0305	1/2	16.9	833	Nonuniform
11	.0304	1/2	11.85	910	Nonuniform
12	.0301	1	25.1	400	Nonuniform
13	.0311	1	19.2	635	Nonuniform

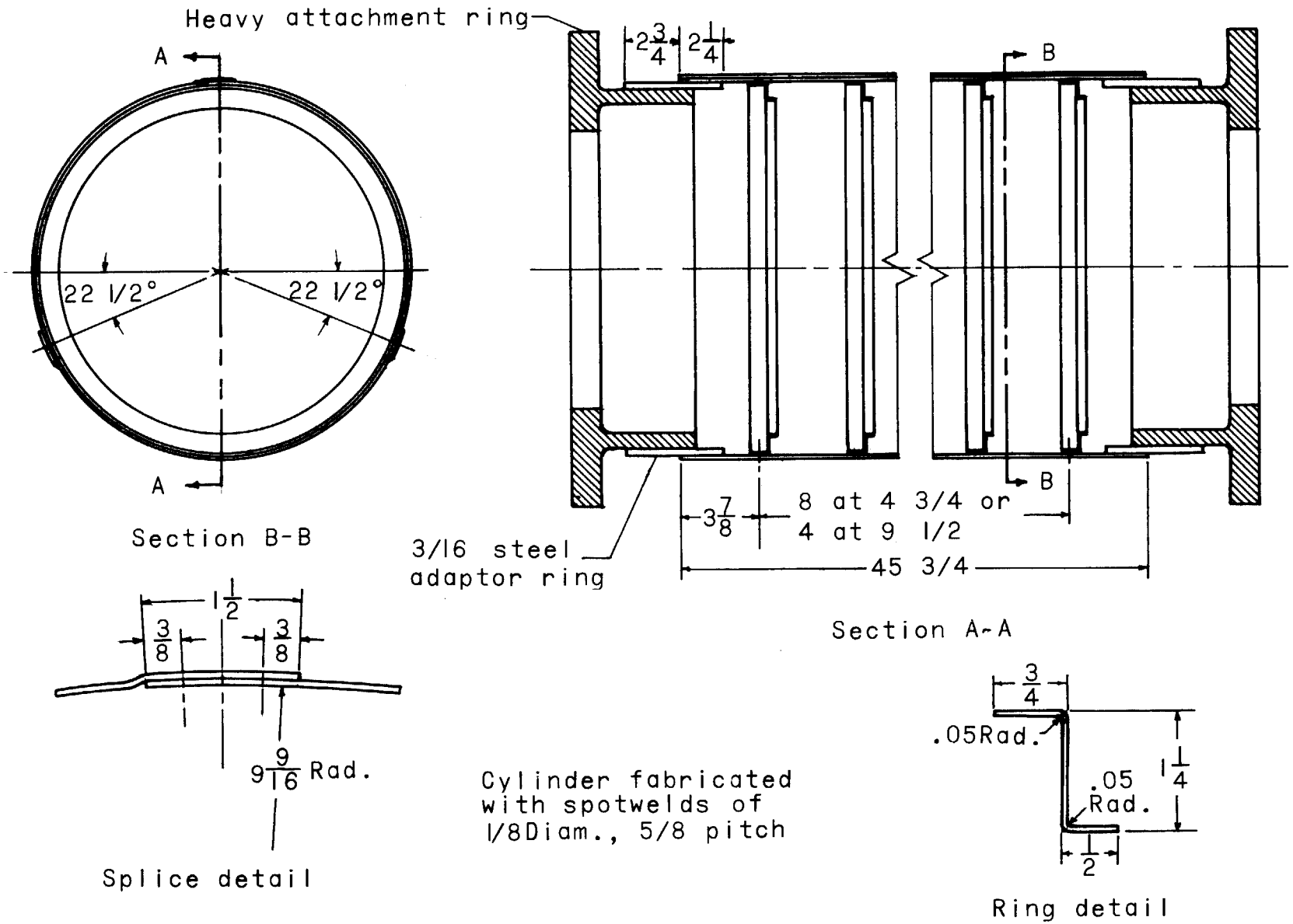

Figure 1.- Fabrication details for ring-stiffened-cylinder test specimens. (All dimensions are in inches unless otherwise indicated.)

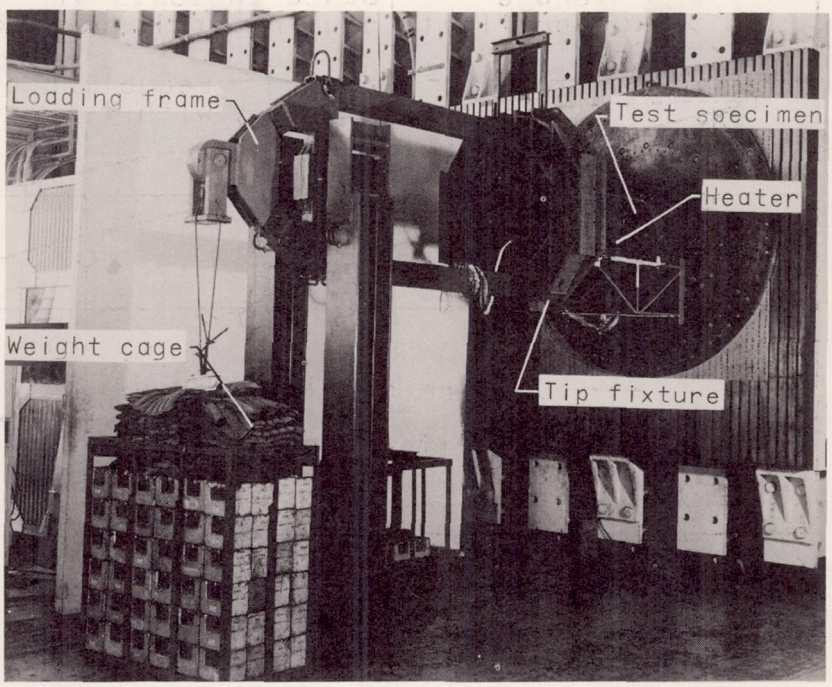

(a) General view of test setup. L-61-6326.1

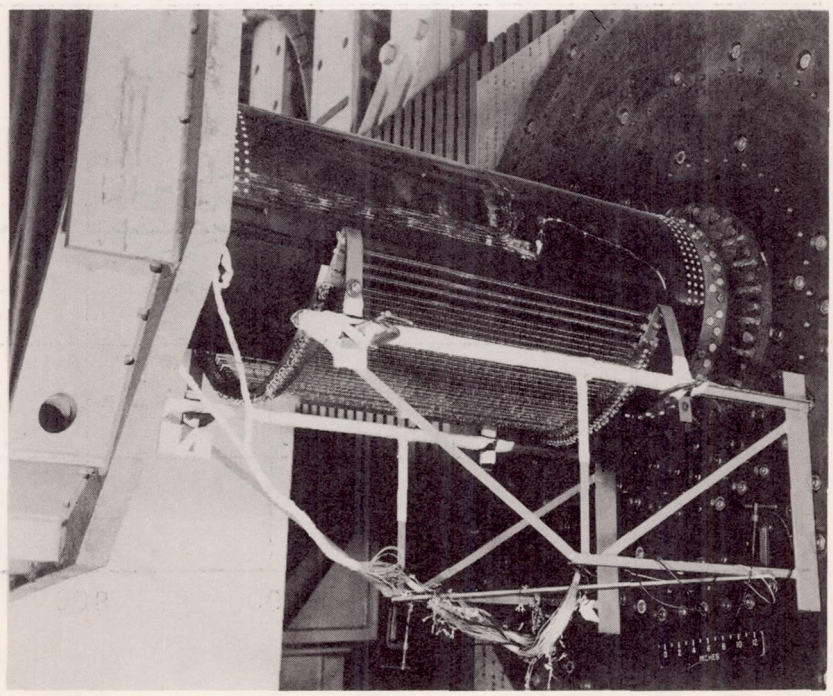

(b) Detail view of heater installations. L-61-6327

Figure 2.- Method of loading and heating test cylinders.

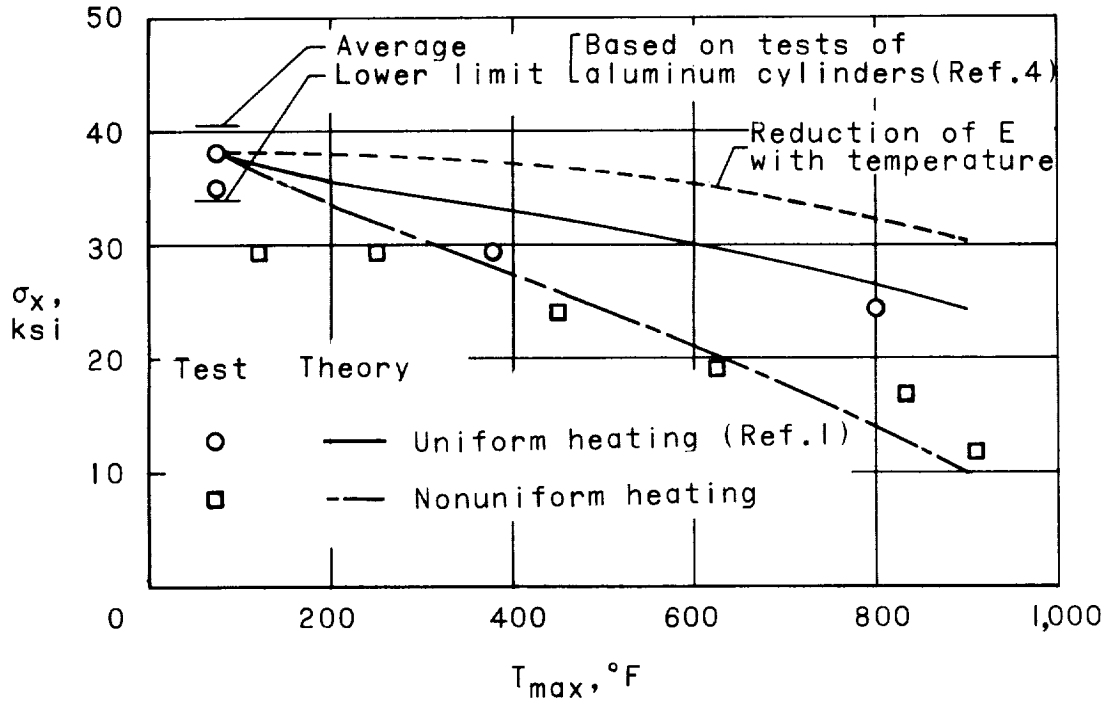

(a) L/R = 1/2.

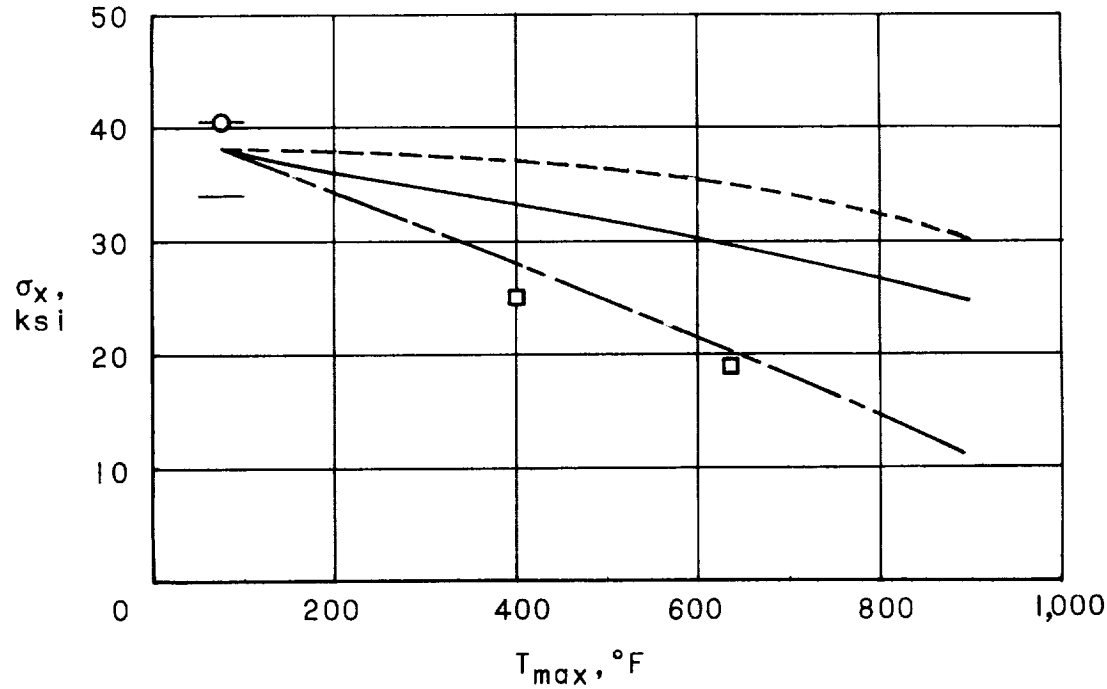

(b) L/R = 1.

Figure 3.- Test results for cylinders loaded in pure bending and rapidly heated.

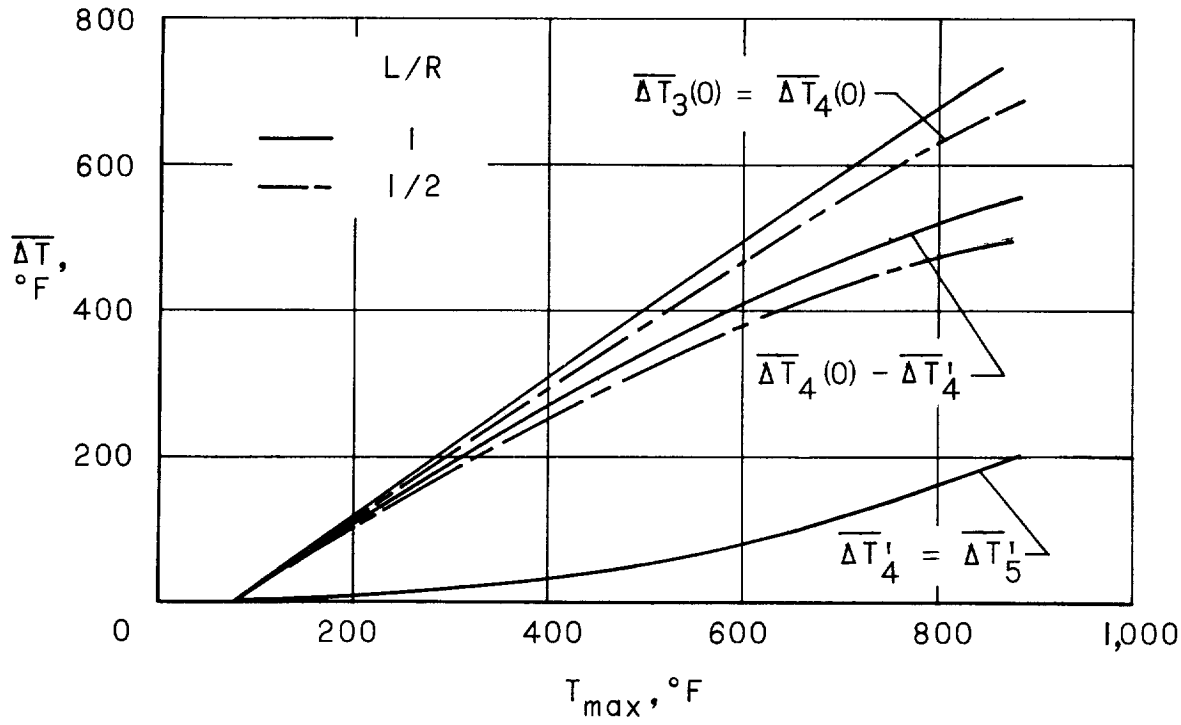

Figure 4.- Variation of average skin and ring temperatures with maximum cylinder temperature.

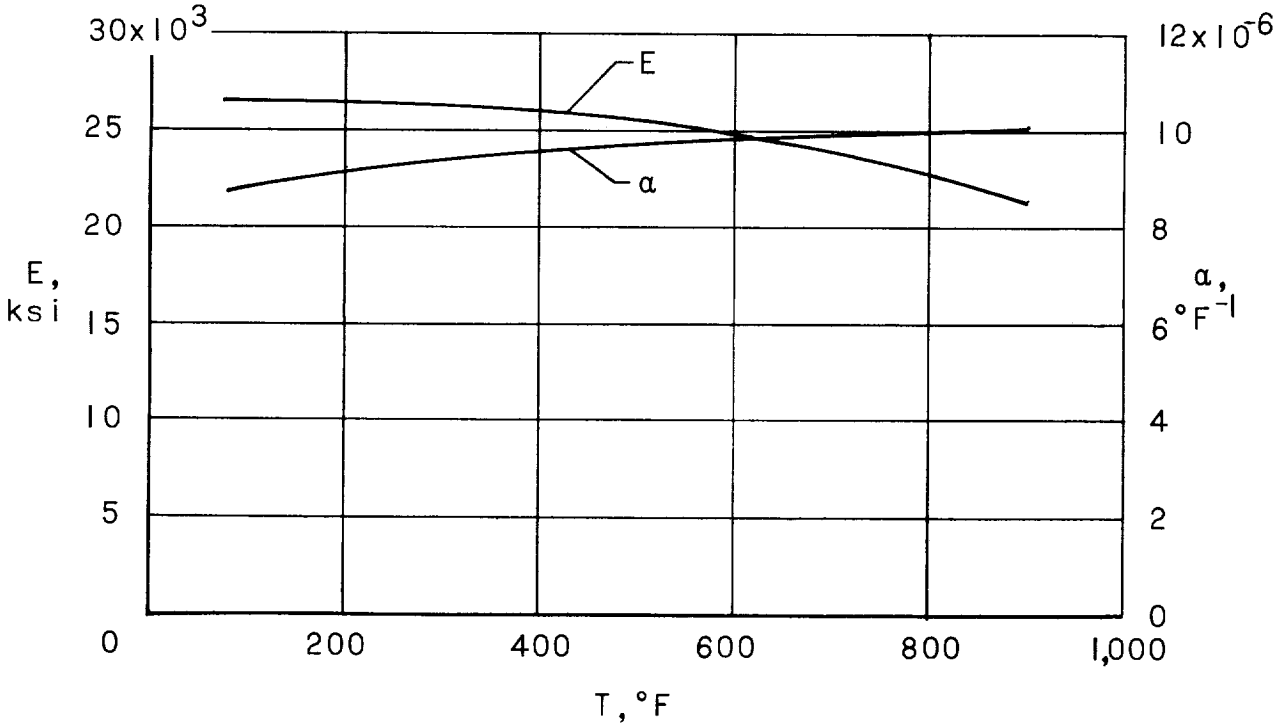

Figure 5.- Variation of α and E with temperature for 301 stainless steel.

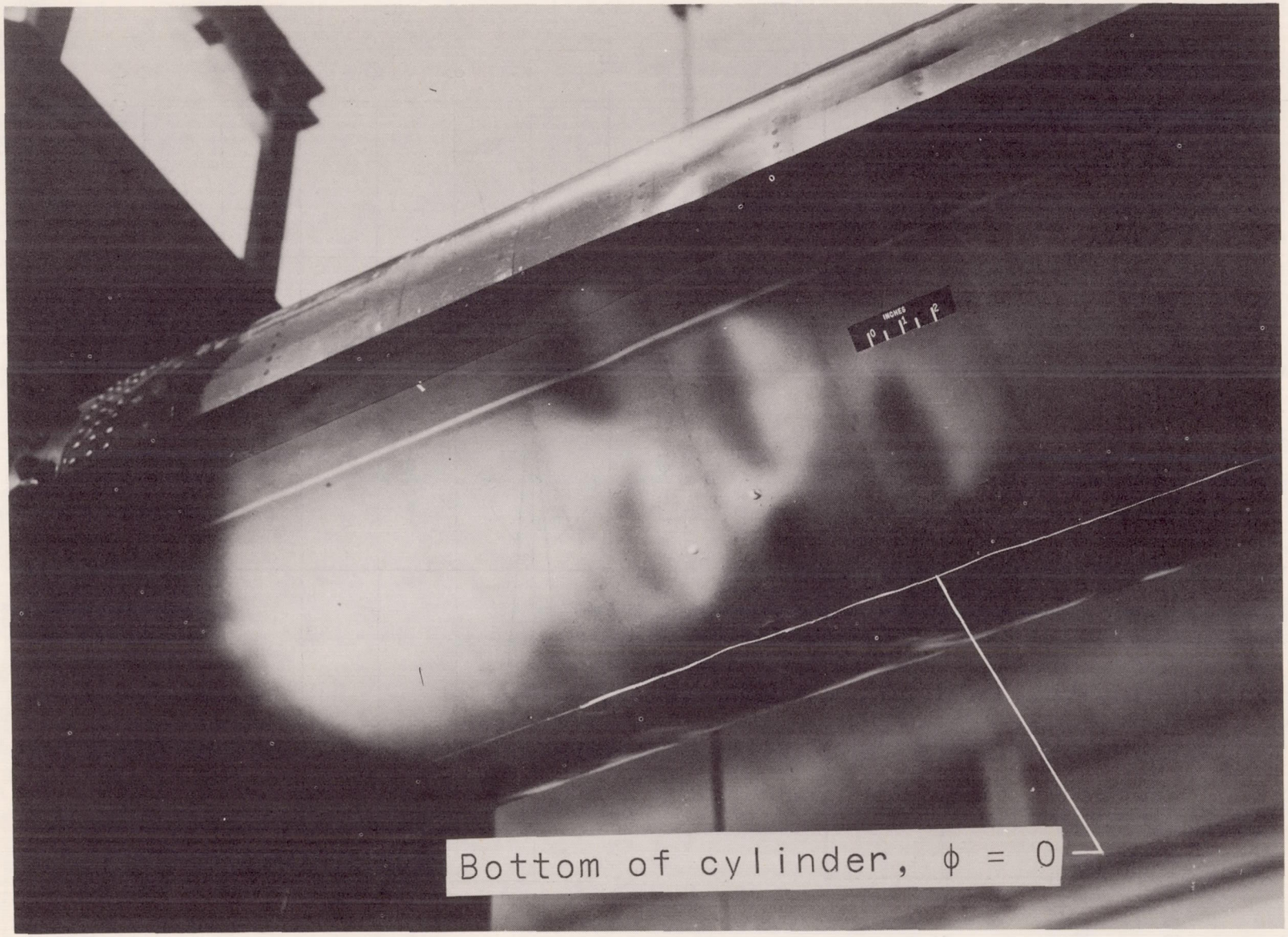

Figure 6.- Buckle pattern for cylinder 9. L-60-344

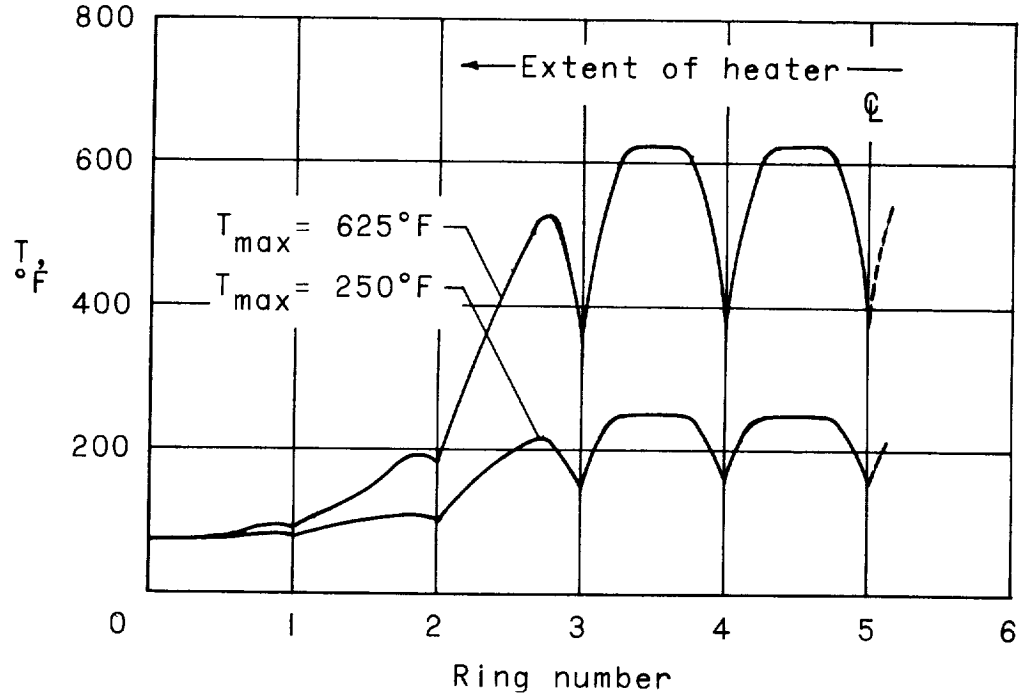

Figure 7.- Typical experimental longitudinal temperature distribution. $\phi = 0$; $\frac{L}{R} = \frac{1}{2}$.

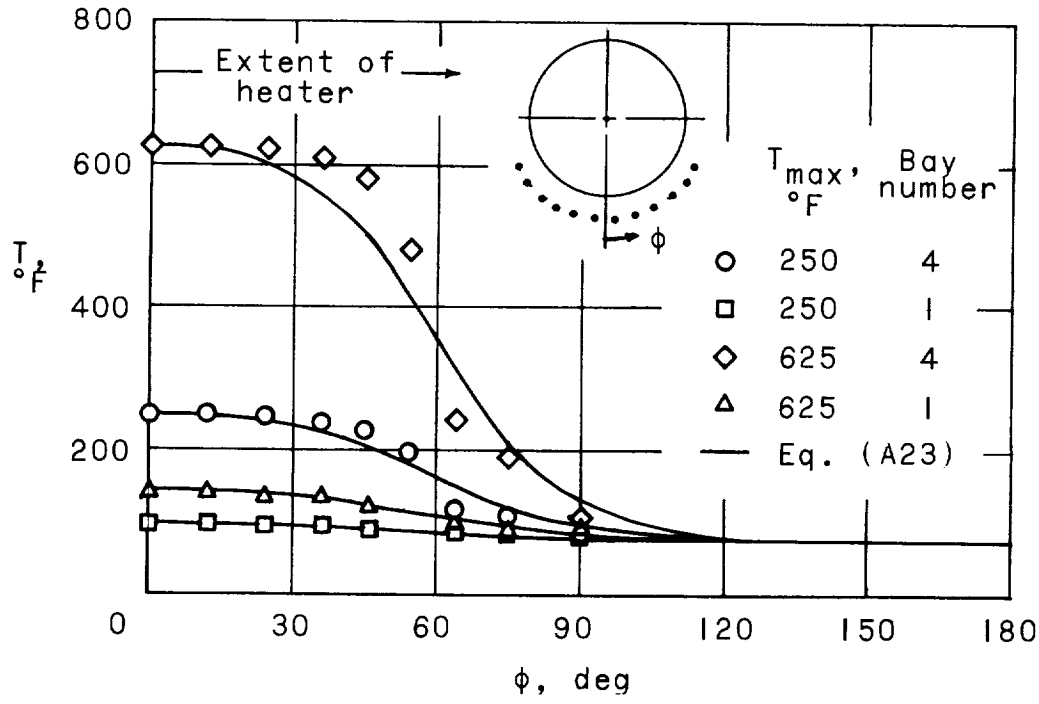

Figure 8.- Typical circumferential temperature distribution at midbay.

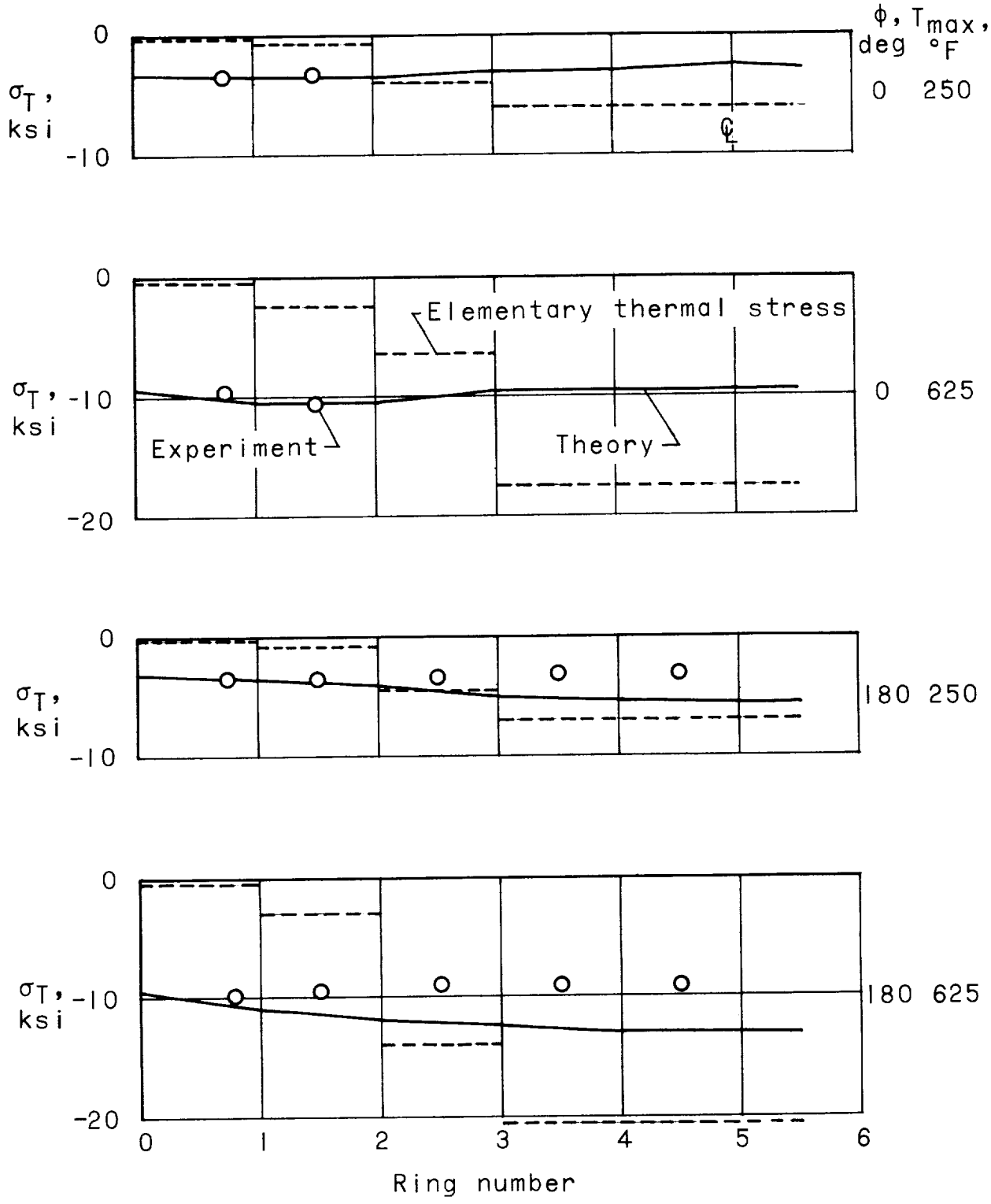

(a) Variation of axial thermal stress in longitudinal direction.

Figure 9.- Comparison of theoretical and experimental thermal stresses.

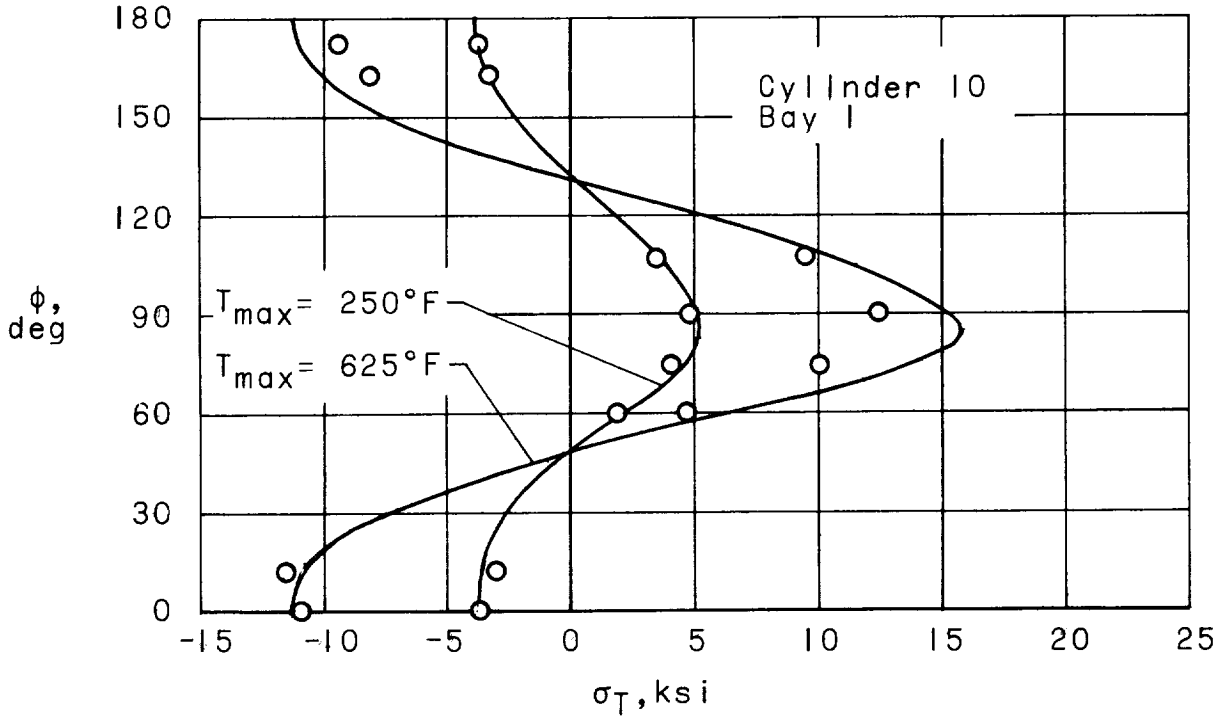

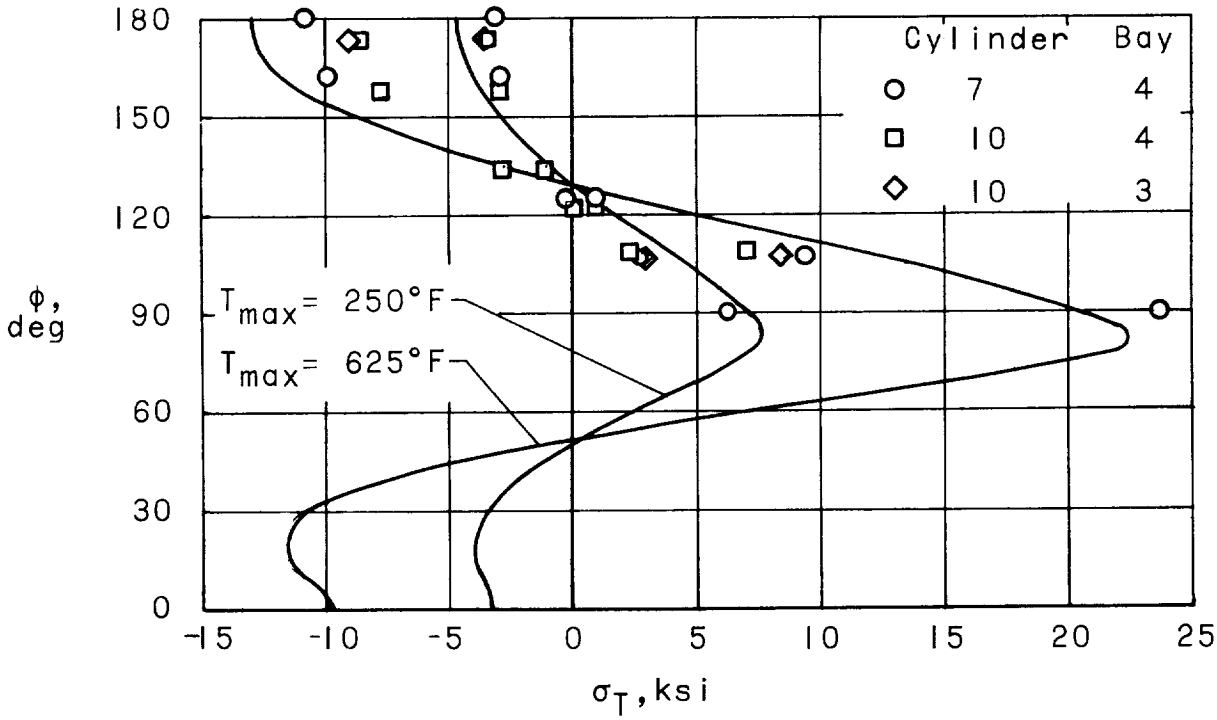

(b) Variation of axial thermal stress in circumferential direction.

Figure 9.- Concluded.

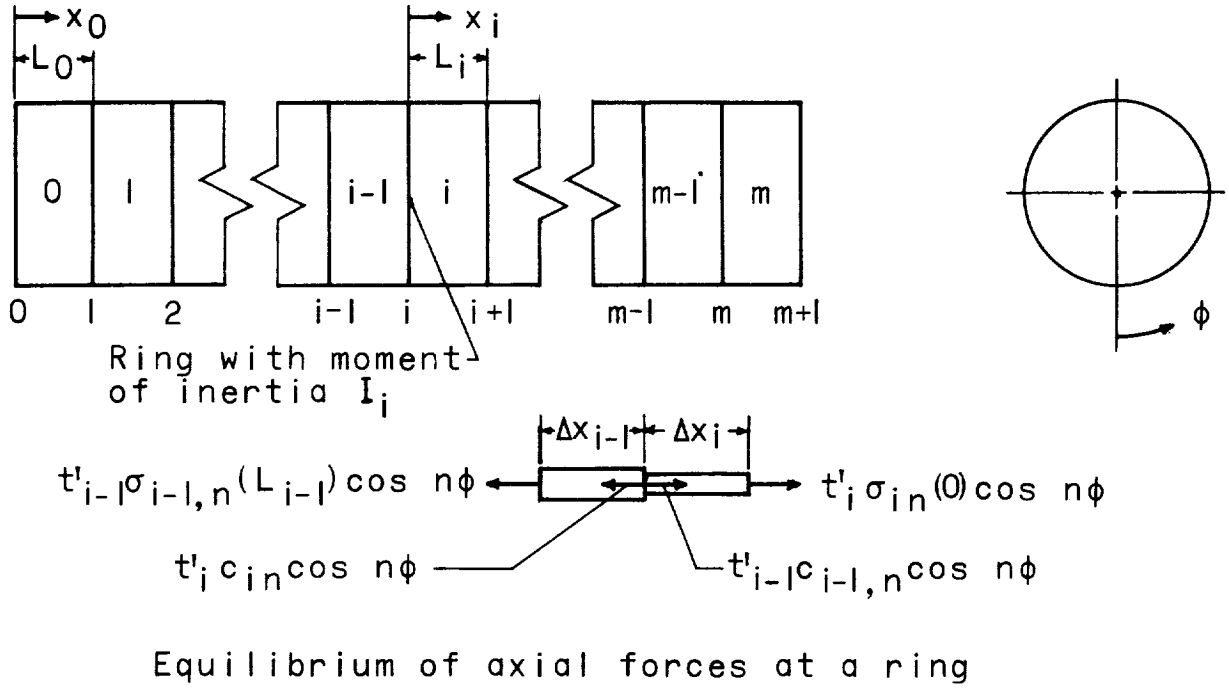

Figure 10.- Cylinder coordinate system with bay and ring numbering system.

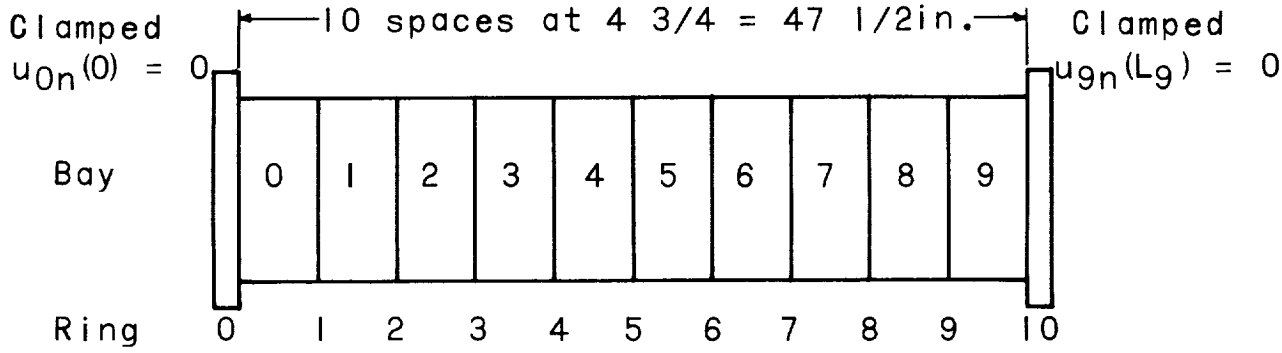

$I_0 = I_{10} = \infty$

$t' = t = 0.0306$in.

$R = 9.56$in.

For $L/R = 1/2$

$I_i = 0.0295$ in.^{4}

For $L/R = 1$

$I_i = 0.0295$ in.^{4} (i = odd)

$I_i = 0.000113$ in.^{4} (i = even)

Figure 11.- Idealization of test cylinders for analysis.

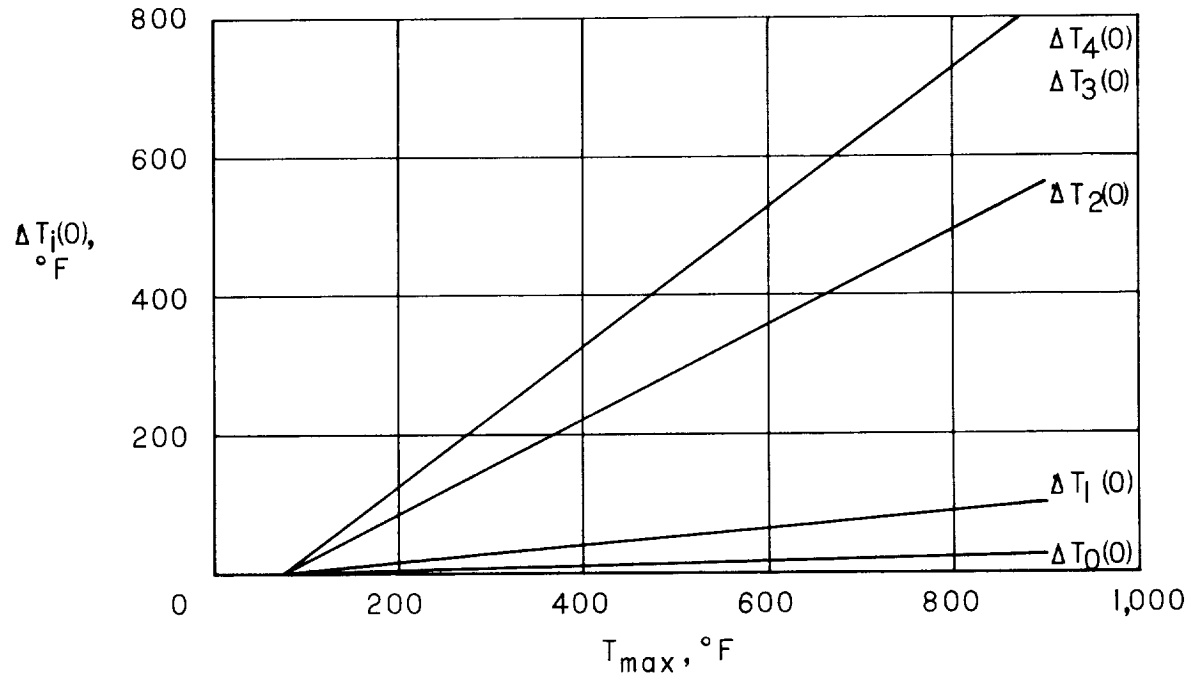

(a) Temperature rise at midbay.

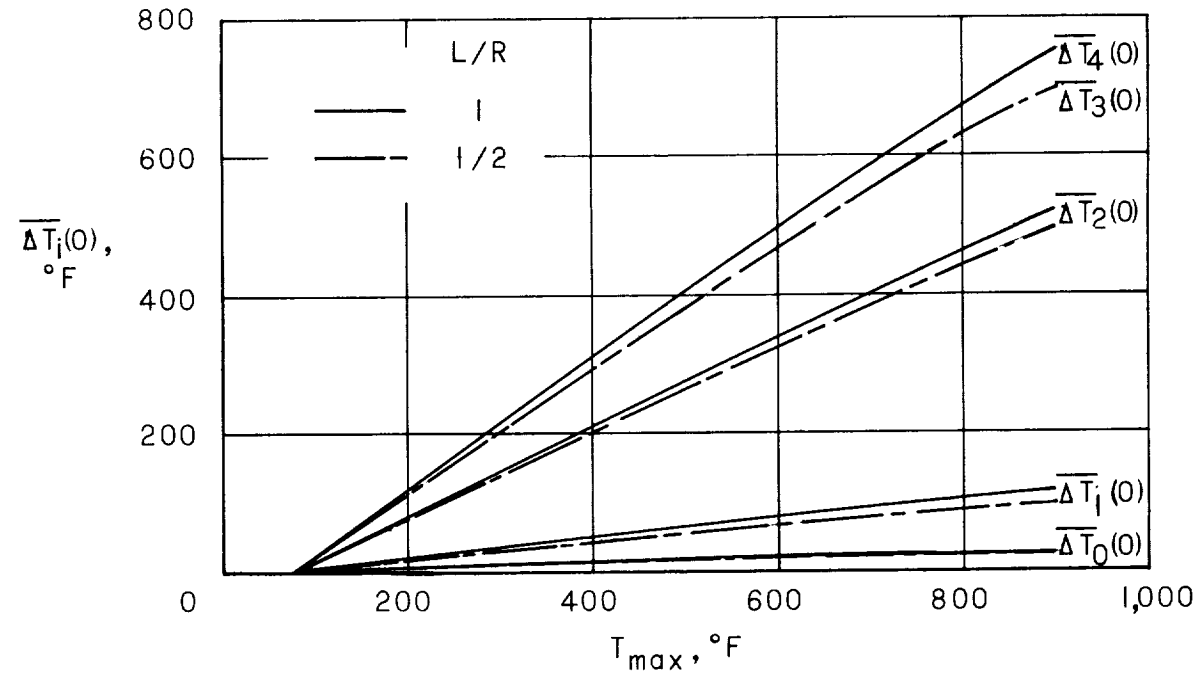

(b) Average temperature rise.

Figure 12.- Variation of temperature rise at bottom of cylinder with maximum cylinder temperature.

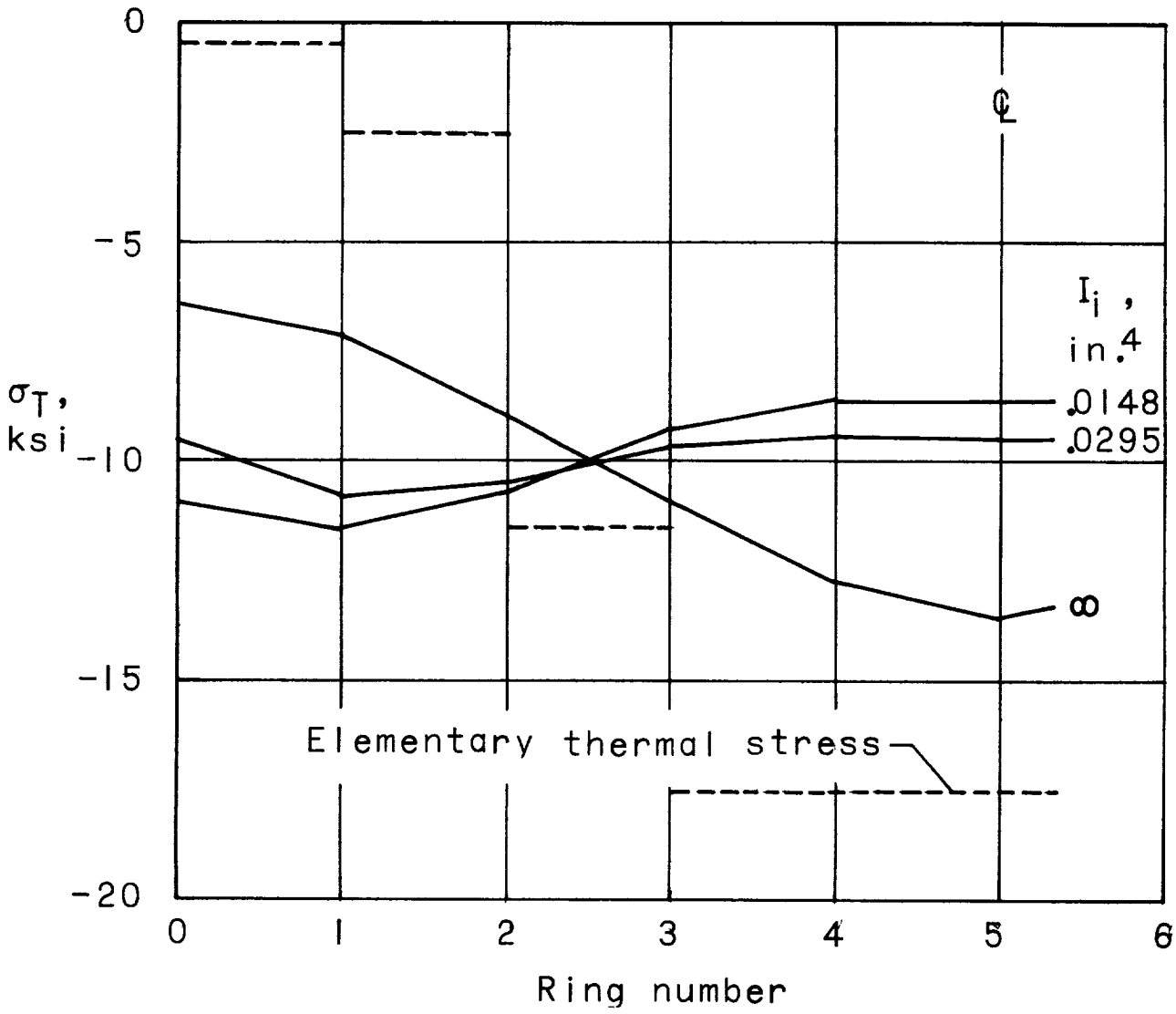

Figure 13.- Effect of ring moment of inertia on cylinder thermal stress. $\phi = 0$; $T_{max} = 625^{\circ}$ F.

NASA-Langley, 1962 L-3153